Annals of Nuclear Medicine **2009, 23(9): 821-827**

COMPARISON BETWEEN REBINNING METHODS AND CLASSICAL GEOMETRIC RE-PROJECTION FOR THE ESTIMATION OF MISSING OBLIQUE DATA IN 3D PET

F Ben Bouallègue, JF Crouzet, and D Mariano-Goulart

Abstract

Objective – Classically, the missing portions in the oblique projection data acquired from cylindrical scanners are synthesized by forward projecting an estimation of the activity computed from non-oblique data. Another quick and powerful way to perform the estimation of the truncated portions consists in applying Fourier rebinning methods. This paper intends to compare the performances of 3D geometric re-projection versus two Fourier rebinning techniques (iterative FOREPROJ and extended FORE) designed for re-projection.
Methods –Both analytical and noisy 3D projection data corresponding to a phantom constituted of warm and cold ellipsoids over a uniform background are simulated numerically for the SIEMENS Hi-Rez scanner. The object is reconstructed using 3D filtered back-projection. A prior estimation of the missing oblique data is performed using the three algorithms.
Results – The resolution properties and noise behavior of the three methods are compared and demonstrate a significant signal to noise ratio improvement using rebinning based algorithms.
Conclusions – We show that iterative FOREPROJ provides projection data with high accuracy in 60% less time than geometric re-projection.

Keywords

Image reconstruction, positron emission tomography, Fourier rebinning, re-projection.

1. Introduction

Most of the three-dimensional positron emission tomography (3D-PET) scanners actually used in routine clinical practice are characterized by a large axial field of view (FOV) and hence by a wide range of oblique angles for the detected photon pairs. However, the cylindrical geometry of the PET scanners leads to the truncation of the recorded oblique projections. 3D analytic reconstruction methods such as 3D Filtered Back-Projection (3D-FBP) require axial invariance of the processed data to perform the fast Fourier transforms (FFTs) involved. Therefore, the missing oblique data have to be estimated prior to the 3D reconstruction. The classical method for the computation of the missing data consists in a first two-dimensional reconstruction (2D-FBP) using the axially invariant non-oblique projections followed by a 3D geometric re-projection (3D-GP) of the reconstructed object [1].
In a previous paper [2], we described two new re-projection algorithms based on iterative or extended rebinning methods (iterative FOREPROJ: IT-FP, and extended FORE: EX-FP). We showed that these algorithms provide better sinogram estimations and image reconstructions than the classical FOREPROJ and reverse FORE proposed by Defrise *et al* [3,4] although the FORE approximation show evident limitations at high tilt angles.

However, these two new algorithms have not yet been directly compared to the classical 3D-GP method within the frame of 3D direct PET reconstruction. Thereby, the present paper addresses the comparison between the rebinning based projectors IT-FP and EX-FP, and the classical 3D-GP with a volume model. The three methods are compared on numerically simulated data before image reconstruction using 3D-FBP.

2. Materials and Methods

2.1. Theoretical Background

The integral of a radioactive distribution *f(x,y,z)* along the line of response (LOR) parametrized by a radial (*s*), an angular (ϕ), an axial (*z*) and a co-polar (θ) variables writes (Figure 1):

$$p(s,\phi,z,\delta)=\int_{-\infty}^{+\infty} dt \;\; f\,(\,s\cos\phi - t\sin\phi\,,\;\; s\sin\phi + t\cos\phi\,,\, z + t\,\delta\,) \qquad (1)$$

where $\delta = \tan\theta$. A set of projections with constant co-polar angle θ is called a segment and is indexed from 0 (θ = 0) to N ($\theta = \theta_{max}$).

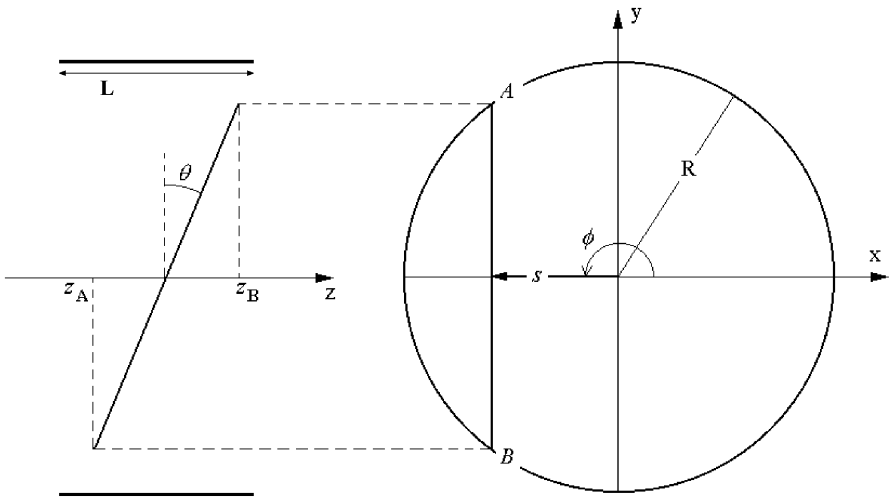

Fig. 1 Geometry of a PET scanner. *Left*: longitudinal section showing the axial variables *z* and θ. *Right*: transaxial view. The standard sinogram variables *s* and ϕ parameterize the straight line AB

Due to the cylindrical geometry of the scanner, the coincidences are recorded for a given copolar angle in the range (Figure 2):

$$|\,z\,| \le \frac{L}{2} - \delta\, R \qquad (2)$$

with *R* the radius of the field of view of the PET scanner.
However the projection information lies all over the range:

$$|\,z\,| \le \frac{L}{2} + \delta\, R \qquad (3)$$

Thus the truncation affects the data in the range:

$$\frac{L}{2} - \delta\, R < |\,z\,| \le \frac{L}{2} + \delta\, R \qquad (4)$$

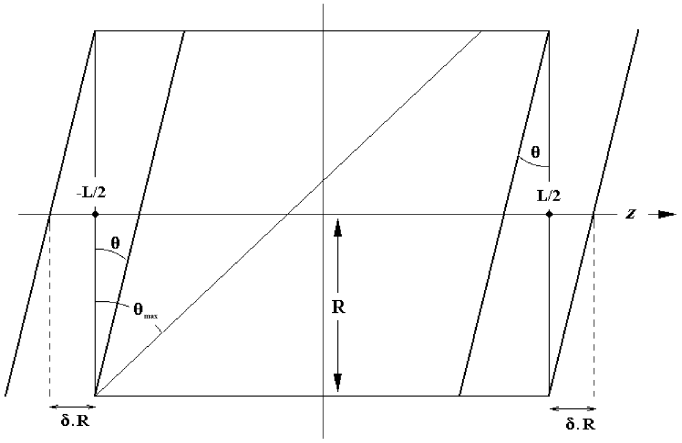

Fig. 2 The problem of the missing projections in the set of measured data: only segment 0 ($\delta = \tan\theta = 0$) is axially invariant. Here, $\theta_{max} = \text{atan}(\delta_{max})$ is the aperture of the scanner, with δ_{max} the maximum ring difference

Only segment 0 ($\theta = 0$) is axially invariant. Upper segments ($\theta > 0$) must be completed before the application of 3D-FBP. Our goal is to compare the three following methods for the completion of the oblique 3D data (Figure 3):

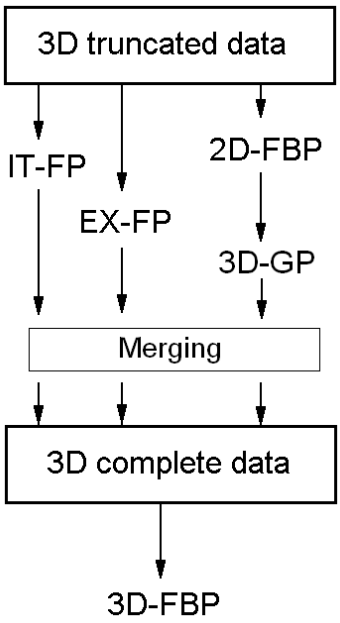

Fig. 3 Diagram for the comparison of the three re-projection methods

2.1.1. Geometric re-projection

The 3D geometric re-projection (3D-GP) is performed on the basis of a slice-by-slice reconstruction of the object realised with the non-oblique projections by means of a 2D-FBP for each transaxial slice [1]. Denoting f^* the first estimation of the activity f, the missing projections are computed using a geometric projector GP(L,i,j,k):

$$p(s, \phi, z, \delta) = \sum_{i,j,k} \text{GP}(\text{L, i, j, k}) \; f^*(\text{i, j, k}) \qquad (5)$$

where the summation runs over the voxel indices (i,j,k) and the index L represents the LOR with parameters (s,ϕ,z,δ). The components of the GP matrix represent the volume of the intersection between the voxel (i,j,k) and the LOR L. It should be noted that the GP matrix is highly sparse, as a given LOR

only intersects few of the object voxels. The re-projection algorithm is hence designed to optimize the implementation of equation (5) by targetting the non-zero coefficients before the summation.

2.1.2. Iterative FOREPROJ (IT-FP)

The IT-FP method [2] is based on the relation between the 3D Fourier transforms of $p(s,\phi,z,\delta)$ with respect to the first three variables for two different values of δ:

$$\wp(\omega_1, k, \zeta, \delta_1) = \exp(-i\,\Delta\Phi)\ \wp(\omega_2, k, \zeta, \delta_2) \tag{6}$$

$$\omega_1^2 + \zeta^2\,\delta_1^2 = \omega_2^2 + \zeta^2\,\delta_2^2 \tag{7}$$

with

$$\Delta\Phi = k\,(\operatorname{atan}\left(\frac{\zeta\,\delta_1}{\omega_1}\right) - \operatorname{atan}\left(\frac{\zeta\,\delta_2}{\omega_2}\right)) = k\,\operatorname{atan}\left(\zeta\frac{\delta_1^2 - \delta_2^2}{\delta_1\omega_1 + \delta_2\omega_2}\right) \tag{8}$$

Equation (6) allows the iterative estimation [2] of a missing oblique projection $p(s,\phi,z,\delta)$ given the set $\{p(s,\phi,z,\delta'),\ \delta' < \delta\}$ (Figure 4). No radial zero-padding is carried out when applying IT-FP.

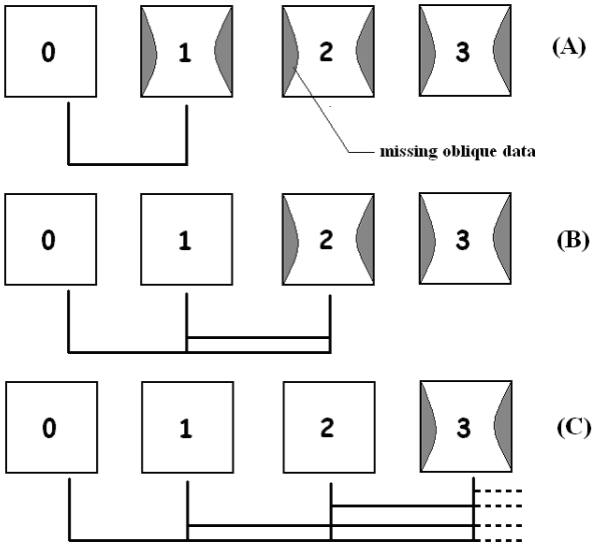

Fig. 4 Flowchart for the computation of IT-FP: segment 1 is first estimated and completed using segment 0 (A). Then segment 2 is completed using segment 0 and 1 (B), and the process goes on iteratively until the every segments has been completed (C)

2.1.3. Extended FORE (EX-FP)

The EX-FP algorithm [2] links every two segments in the 2D Fourier space:

$$P(\omega, k, z, \delta_1) \approx P(\omega, k, z - \frac{k(\delta_1 - \delta_2)}{\omega}, \delta_2) \tag{9}$$

It enables a re-evaluation of any segment on the basis of the entire 3D data set by averaging the right member of equation (9) over the whole δ range.

2.2. Numerical simulations

For the simulations, we choose a phantom constituted of warm and cold ellipsoids over a uniform background (Figure 5). The background activity, fixed to 2, is confined into a cylinder of radius 150 mm. A pattern made up of a centered cold ellipsoid of half-axes 60×60×8.3 mm (activity 1) and eight

off-axis warm ellipsoids of half-axes 20×20×8.3 mm (activity 4) is repeated every 22.8 mm along the *z* axis.

The 3D projection data are simulated analytically [5], assuming no attenuation and equidistant parallel projections, for the SIEMENS Hi-Rez scanner, which is approximated as a 39 ring-scan with a diameter of 823 mm. Each ring is made up of 624 deterctors of size 4 mm. The axial field of view (FOV) is 161.85 mm and the transverse FOV radius is 321.6 mm. The maximum ring difference is fixed to 31 and the axial compression (span) to 3, hence leading to an aperture of 8.6° and eleven values for the azimutal tilt angle θ of the recorded coincidences (11 segments, segment 0 corresponding to the transverse projections).

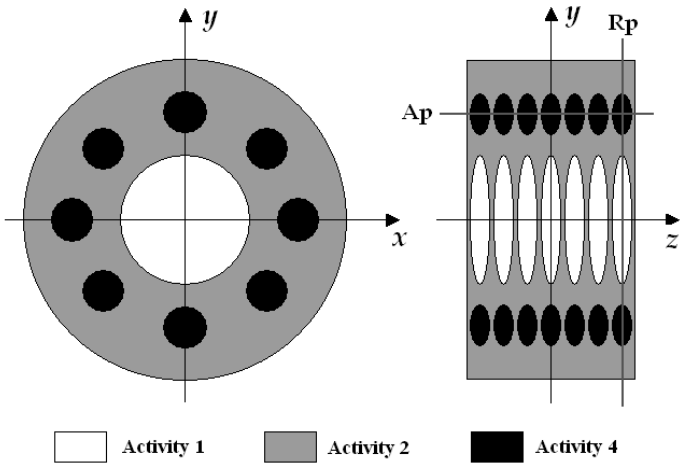

Fig. 5 The studied object is constituted of warm and cold ellipsoids over a uniform background. Here are displayed the (*x*,*y*) and the (*y*,*z*) views

The initial sampling of the 2D sinograms for the SIEMENS Hi-Rez scan is 312×312. These sinograms are re-sampled to 128×128 in order to carry out the FFTs, which leads to a pixel size of 5×5 mm². The axial sampling is conserved: the transverse projections are constituted of 77 slices, which correspond to a slice thickness of 2.075 mm. Zero-padding is achieved in the axial direction in order to bring the number of samples to 128.

Besides the noiseless simulation, Poisson noise is introduced into the data [5] in order to study the noise behavior of the algorithms. The total of the simulated net trues range 100-400 Mcounts. In these two sets of projections, the noiseless ones and the the noisy ones, there are missing oblique data, as the software only simulates the data really acquired by the scanner.

In order to judge the quality of the three methods in estimating these missing oblique data, we analytically compute the whole set of complete 3D projections, called in what follows 'exact data'.

The oblique projections corresponding to segments 1 to 10 are estimated for both noiseless and noisy data using the three methods. Concerning 3D-GP, the prior 2D-FBP reconstruction is performed using a ramp filter implemented either with a cut-off at 60% of the Nyquist frequency or without cut-off. These two implementations are respectively referred to in what follows as 3D-GP-60% and 3D-GP-100%. The estimated oblique projections are compared with the exact data for segments 2, 6 and 10.

After the estimation stage, the calculated projections are merged with the simulated ones in the range $|z| > L/2 - \delta R$. The completed data are then used to run 3D-FBP. When processing noisy data, the frequency cut-off of the Colsher filter is fixed to 60% of the Nyquist frequency. When processing noiseless data, no cut-off is applied to the Colsher filter.

When performing 2D or 3D-FBP, the image matrix has a size of 128×128×128 corresponding to a voxel size of 5×5×2.075 mm^3.

3. Results and discussion

Figures 6 and 7 show the histograms of the pixel difference (in absolute value) between the exact sinograms and the sinograms estimated (computed from the whole sinograms, before merging) from both noiseless (Fig. 6) and noisy (Fig. 7, 200 Mcounts) data. Figure 6 shows that IT-FP provides estimations whose quality in terms of absolute error is comparable to that achieved with 3D-GP, whatever the segment considered. Due to the approximations involved, the results of EX-FP remain acceptable for the first segments but quickly deteriorate with the copolar angle of the computed projections. Figure 7 shows clearly that the data estimated with EX-FP and IT-FP are more reliable than those estimated with 3D-GP-100% when working with realistic noisy data. The quality of the sinograms computed with the rebinning methods is equivalent to that achieved with 3D-GP-60%. Due to the iterative implementation, the results obtained with IT-FP tend to improve with the segment index. Inversely, because of an increasing systematic error, the quality of the EX-FP estimations decreases with the segment index.

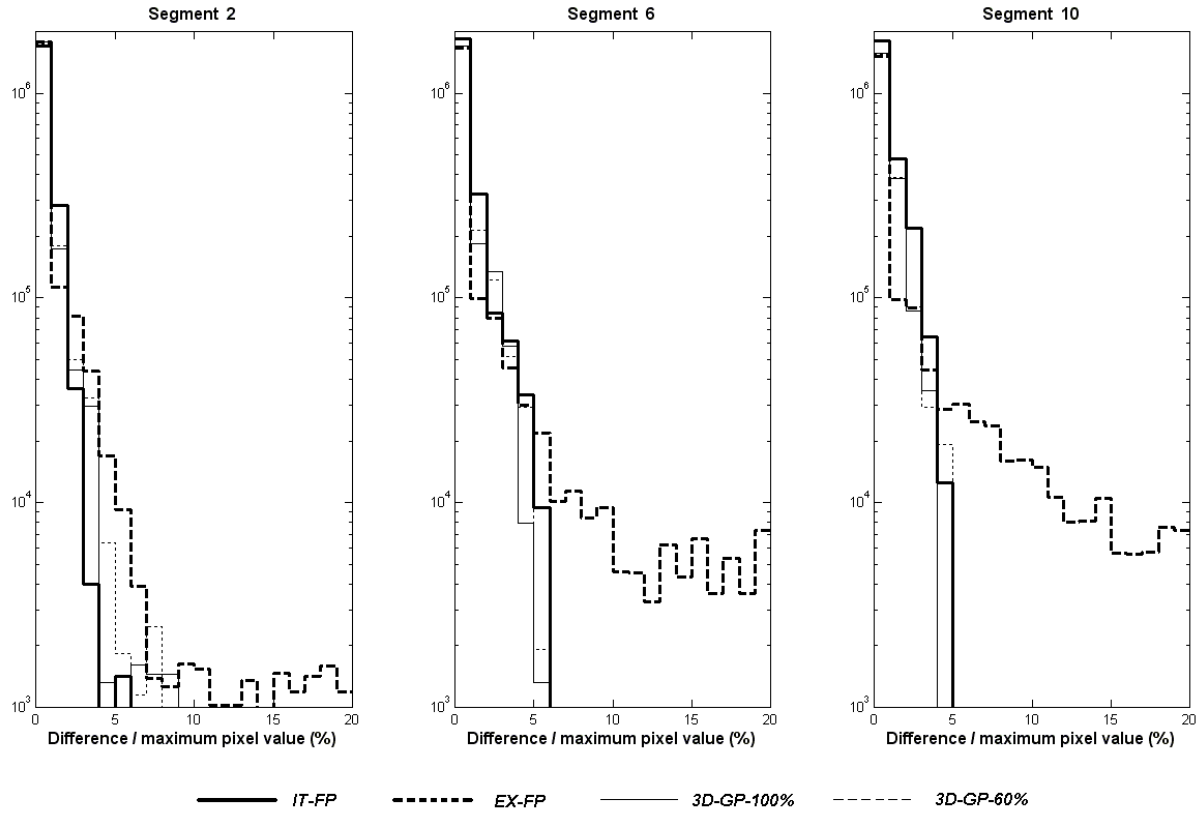

Fig. 6 Histogram of the difference (normalized to the data maximum) between the exact sinograms and the sinograms estimated from noiseless data. Comparison between 3D-GP-60% (dashed), 3D-GP-100% (solid), EX-FP (dashed bold) and IT-FP (solid bold)

Figure 8 shows radial (left) and axial (right) line profiles through the object reconstructed from noiseless data and exhibits the intrinsic influence of each method on the spatial resolution. The profiles are respectively extracted through line *Rp* and line *Ap* shown on Figure 5. They attest that there is no resolution loss when using IT-FP compared with the resolution recovery achieved with 3D-GP. Moreover, the axial line profiles show that IT-FP leads to fewer partial volume effects in the external slices. As for EX-FP, it exhibits axial smoothing due to axial interpolations following from equation (9), as well as radial distortions following from the bad quality of the upper segments estimation.

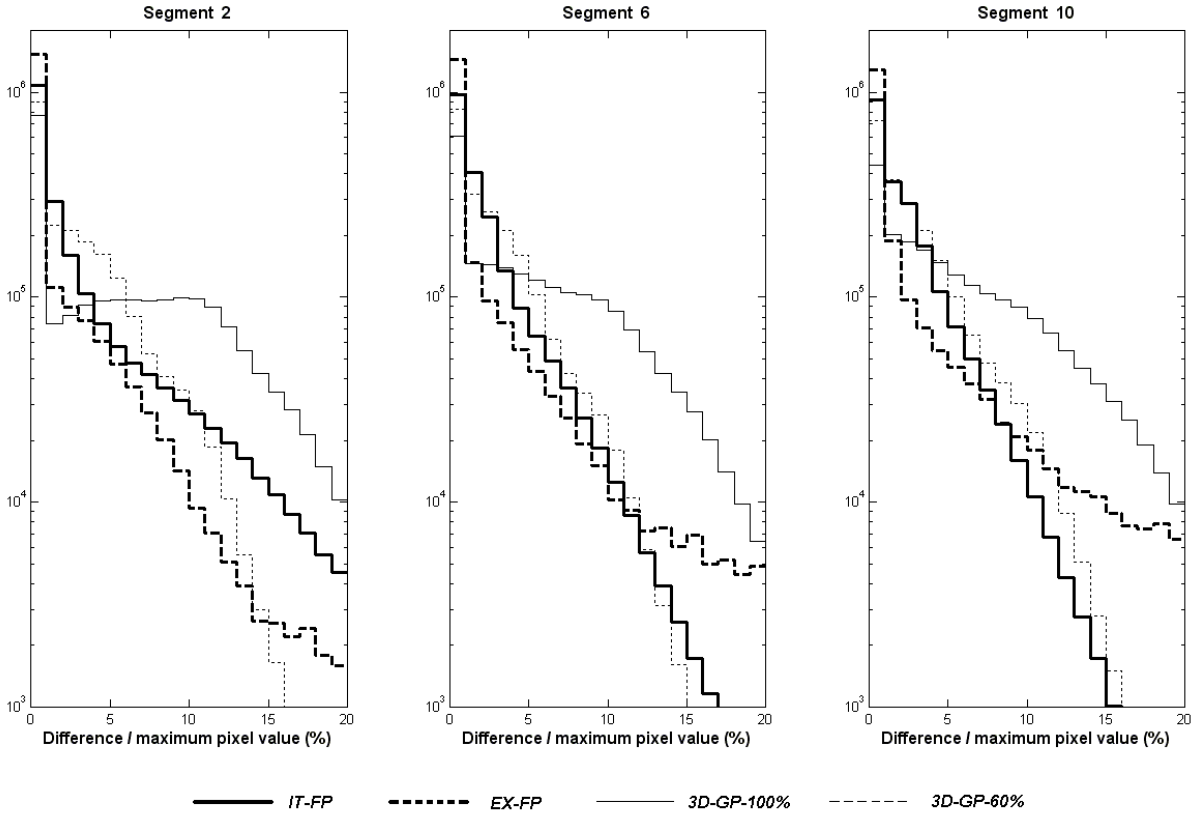

Fig. 7 Histogram of the difference (normalized to the data maximum) between the exact sinograms and the sinograms estimated from noisy data (200 Mcounts). Comparison between 3D-GP-60% (dashed), 3D-GP-100% (solid), EX-FP (dashed bold) and IT-FP (solid bold)

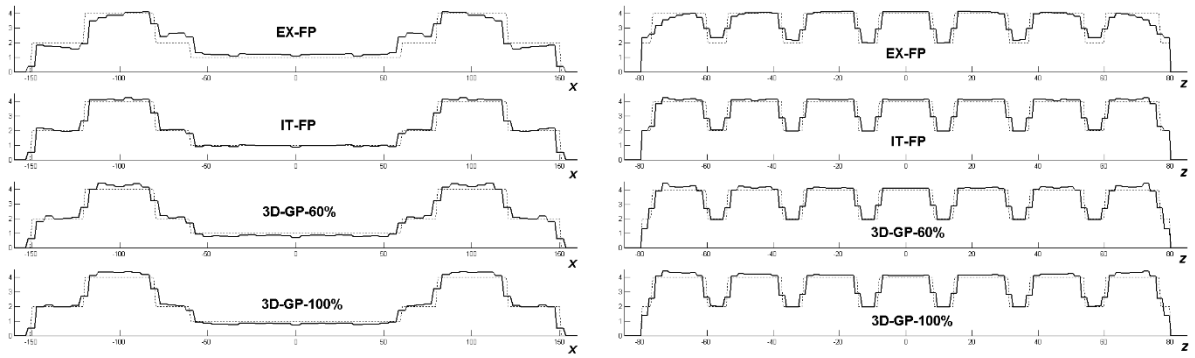

Fig. 8 Radial *(left)* and axial *(right)* line profiles through the object reconstructed from noiseless data. The dashed curves correspond to the exact line profile through the object. The completion was achieved using, from top to bottom: EX-FP, IT-FP, 3D-GP-60% and 3D-GP-100%

Figure 9 illustrates the noise performance of the three methods by comparing the relative standard deviation (in %) in the reconstructed warm ellipsoids. For a given slice, the standard deviation is averaged over the eight ellipsoids centered on the slice and normalized to the mean pixel value of the eight ellipsoids. From left to right, the columns correspond respectively to 100, 200 and 400 Mcounts simulated. Whatever the noise level, EX-FP provides significant signal to noise ratio improvement in the reconstructed volumes compared to 3D-GP, due in great part to the approximation involved and the resulting smoothing. IT-FP allows as well a clear relative standard deviation reduction in the external ellipsoids, this reduction increasing with the simulated data statistics: the maximum reduction reaches 7% for 200 Mcounts and 9% for 400 Mcounts.

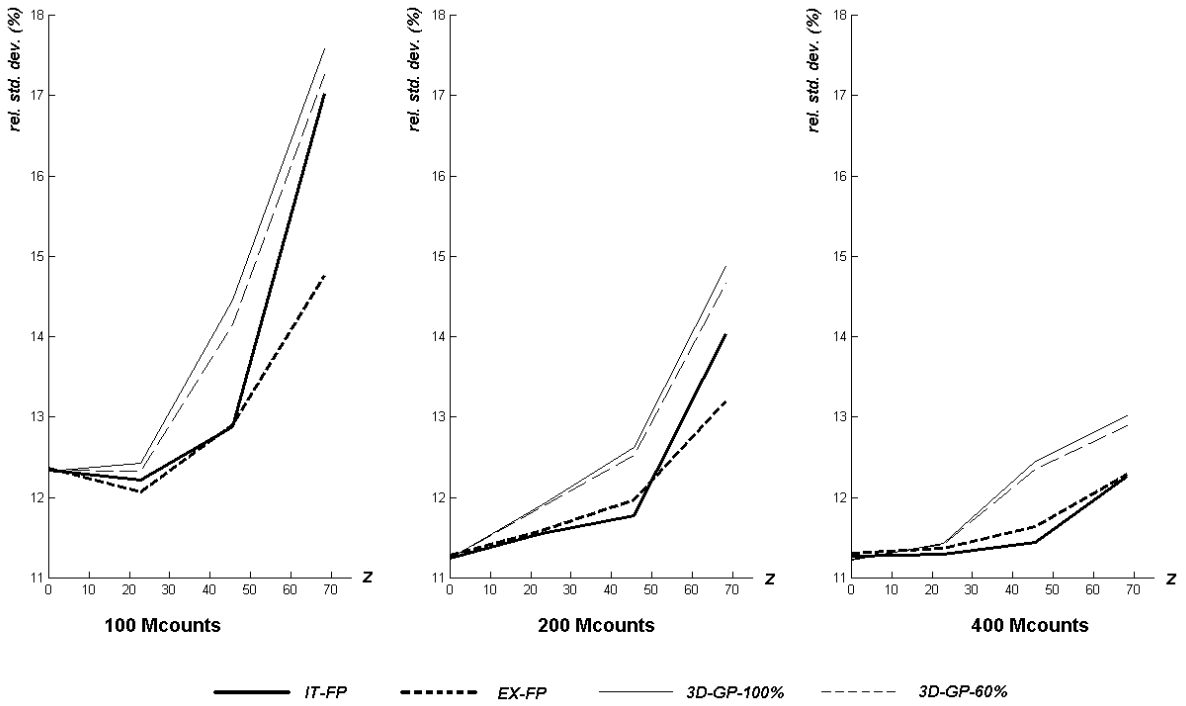

Fig. 9 Relative standard deviation calculated in the reconstructed warm ellipsoids. Completion was performed using 3D-GP-60% (dashed), 3D-GP-100% (solid), EX-FP (dashed bold) and IT-FP (solid bold). *From left to right*: 100, 200 and 400 Mcounts simulated. The 3D-FPB was implemented with a cut-off at 60% of the Nyquist frequency for the Colsher filter

By way of illustration, Figure 10 shows external slices (z = 68.5 mm) extracted from the reconstructed volumes. Finally, Table 1 illustrates the processing times (with a 3 GHz personal computer) of each method for the considered case: SIEMENS Hi-Rez scanner with ten truncated segments and a (s, ϕ, z) sampling of 128×128×128 (after re-sampling in the s and ϕ variables, and zero-padding in the z direction). These times do not include the 3D object reconstruction using 3D-FBP. It does neither include the time for the computation of the GP matrix which is computed once and stored on hard disk for further exploitation. It appears that the processing time is 2.4 longer with 3D-GP than with IT-FP. As analytical reconstructions are chosen generally because they perform faster than iterative methods, the faster execution time of IT-FP followed by 3D-FBP may be of prime importance when fast 3D reconstructions are required.

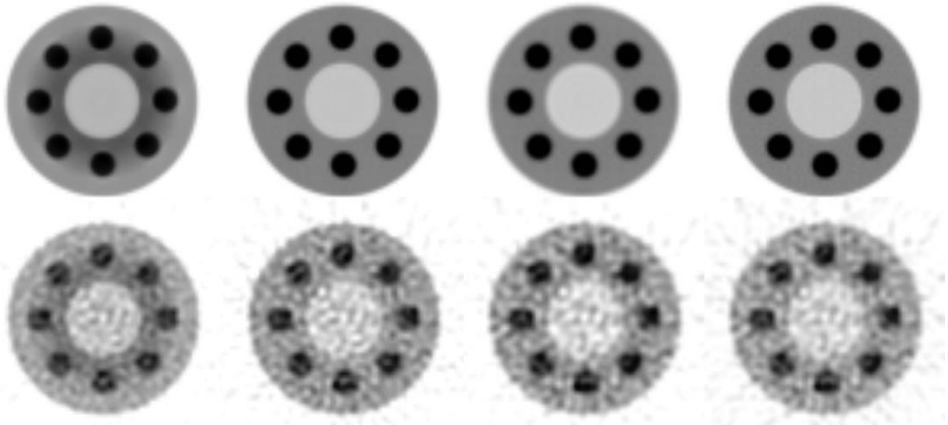

Fig. 10 Volumes reconstructed from noiseless (top) and noisy (bottom) projection data. External transverse slice (z = 68.5 mm). *From left to right:* estimation of the missing data with EX-FP, IT-FP, 3D-GP-60% and 3D-GP-100%. 200 Mcounts. The 3D-FPB was implemented with a cut-off at 60% of the Nyquist frequency for the Colsher filter.

Table 1 Representative computational costs

Method	Computation time
EX-FP	45 sec
IT-FP	120 sec
2D-FBP + 3D-GP	80 sec + 210 sec = 290 sec

4. Conclusions

We performed a systematic comparison between 3D geometric re-projection and two Fourier rebinning algorithms designed for the solution of the data truncation problem (IT-FP and EX-FP), including quality of the estimated segments, resolution properties and noise behavior. EX-FP exhibits significant standard deviation reduction compared with 3D-GP. However, as it implies the same axial approximation as FORE does, it lead to artifacts in the estimated segments resulting in loss of resolution and distortion in the reconstructed volumes. For IT-FP, the quality of the estimated segments is equivalent to that of 3D-GP when working with noiseless data. When working with noisy data, the quality of the estimated sinograms in terms of absolute error is comparable to that achieved with 3D-GP. In addition, IT-FP allows 3D reconstructions with fewer partial volume effects in the external slices and similar axial resolution in 60% less time.

Acknowledgment

The authors would like to thank the anonymous reviewers for their valuable comments and suggestions.

References

[1] Kinahan PE and Rogers JG. Analytic three-dimensional image reconstruction using all detected events. IEEE Trans. Nucl. Sci. 1990; 36: 964-968.

[2] Ben Bouallègue F, Crouzet JF, Comtat C, Fourcade M, Mohammadi B, and Mariano-Goulart D. Exact and approximate Fourier rebinning algorithms for the solution of the data truncation problem in 3D PET. IEEE Trans. Med. Imag. 2007; 26-7: 1001-1009.

[3] Defrise M, Kinahan PE, Townsend DW, Michel C, Sibomana M, and Newport DF. Exact and approximate rebinning algorithms for 3-D PET data. IEEE Trans. Med. Imag. 1997; 16: 145-158.

[4] Liu X, Defrise M, Michel C, Sibomana M, Comtat C, Kinahan PE et al. Exact rebinning methods for three-dimensional positron tomography. IEEE Trans. Med. Imag. 1999; 18: 657-664.

[5] Comtat C, Kinahan P, Defrise M, Michel C, Lartizien C, and Townsend D. Simulating whole-body PET scanning with rapid analytical methods. Proceedings of IEEE Nuclear Science Symposium and Medical Imaging Conference, Seattle, WA, 1999. Piscataway, NJ: IEEE, 2000 M7-83.